Symmetry breaking induced magnon-magnon coupling in synthetic antiferromagnets

Mei Li,[1] Jie Lu,[2,*] and Wei He[3,†]

[1]*Physics Department, Shijiazhuang University, Shijiazhuang, Hebei 050035, People's Republic of China*

[2]*College of Physics and Hebei Advanced Thin Films Laboratory, Hebei Normal University, Shijiazhuang 050024, People's Republic of China*

[3]*State Key Laboratory of Magnetism and Beijing National Laboratory for Condensed Matter Physics, Institute of Physics, Chinese Academy of Sciences, Beijing 100190, People's Republic of China*

(Received 3 November 2020; revised 18 January 2021; accepted 12 February 2021; published 22 February 2021)

We propose a general theory of ferromagnetic resonance (FMR) spectroscopy for symmetry-breaking synthetic antiferromagnets (SAFs). Generally, both inhomogeneity and different thickness of the two ferromagnetic sublayers of a SAF result in the intrinsic symmetry breaking, thus excludes the crossing between pure in-phase and out-of-phase resonance modes with opposite parity. Alternatively, new frequency branches become hybridization of original bare modes in terms of symmetry breaking induced magnon-magnon coupling, hence generate an indirect gap in FMR frequencies. The gap widths for several typical cases are presented and compared with existing data. In particular, for the inhomogeneity case, the indirect gap width is linearly proportional to the asymmetry degree and takes a square (rather than linear) dependence on the magnon-magnon coupling strength, indicating a case-by-case recalibration of the measuring method of the latter. Our theory provides a simple but physical understanding of the rich structure of FMR spectra for asymmetric SAFs.

DOI: 10.1103/PhysRevB.103.064429

I. INTRODUCTION

Synthetic antiferromagnets (SAFs) are magnetic multilayers with two ferromagnetic (FM) sublayers coupled antiferromagnetically through a nonmagnetic metallic spacer [1]. They have attracted tremendous interest in the past decades due to their potential for developing the "SAF spintronics" and wide range of applications in magnetic nanodevices [2–21]. Compared with the strong exchange coupling in genuine antiferromagnetic (AFM) materials with terahertz intrinsic frequencies [22,23], the relatively weak interlayer coupling in SAFs mainly comes from the Ruderman-Kittel-Kasuya-Yosida (RKKY) interaction [24–26] thus realizes gigahertz FM resonance (FMR) frequencies that mature microwave electronics can match. Similar behaviors have also been observed in layered crystals [27,28] and compensated ferrimagnets [29] with AFM interlayer and intersublattice couplings, respectively. More interestingly, for symmetrical NiFe/Ru/NiFe [2,16] and FeCoB/Ru/FeCoB SAFs [18–21], or layered crystal $CrCl_3$ [27], symmetry-protected mode crossings between in-phase and out-of-phase branches of FMR spectra have been observed under in-plane external dc magnetic fields, indicating the absence of coupling between magnons with opposite parity therein.

In fact, this mode crossing can be eliminated in several ways. For symmetrical SAFs [20] or layered crystals [27], extrinsically exerting an oblique dc field will lift the system's rotation-symmetry axis away from the SAF plane, thus breaks the rotation invariance of the hard axis (normal of SAF plane) from magnetostatic interaction. This introduces a magnon-magnon coupling between the original uncoupled modes with opposite parity, hence hybridizes the two modes and generate an anticrossing gap. Very recently, strong magnon-magnon coupling under in-plane dc fields is also proposed by the dynamical dipolar interaction from nonuniform precession of magnetic moments in symmetrical FeCoB/Ru/FeCoB SAFs [18,19]. Besides these externally induced cases, the other strategy is to break the intrinsic symmetry between the two FM sublayers in SAFs. In most existing experiments, the two sublayers are prepared from the same FM materials with different thickness. A frequency gap can be observed even under in-plane dc fields [16,17]. In addition, intrinsic asymmetry should also appear when the two sublayers are made from different FM materials. However, to our knowledge, the corresponding FMR measurements are not yet in the press, which mainly comes from the difficulty in sample preparation.

A lot of theoretical works have been performed to understand the rich structure of FMR spectra in SAFs [4,14–18,20,21,27,29]. Representatively, in 2014, a discrete-lattice approach has been raised for asymmetric NiFe/Ru/NiFe SAFs [17] under in-plane dc fields, where the RKKY interaction, biquadratic exchange coupling and the uniaxial anisotropy at the NiFe/Ru interfaces are all considered. In 2019, based on "macrospin" assumption MacNeill *et al.* proposed a systematic analysis for the gap induction from oblique dc magnetic fields in which only the bilinear RKKY interaction is included [27]. However, they did not consider the intrinsic symmetry breaking (SB) since the sublayers of their system are always symmetrical.

In this work, we demonstrate that intrinsic SB in SAFs is enough to induce strong magnon-magnon coupling, and further results in considerable indirect gaps in FMR spectra.

*jlu@hebtu.edu.cn
†hewei@iphy.ac.cn

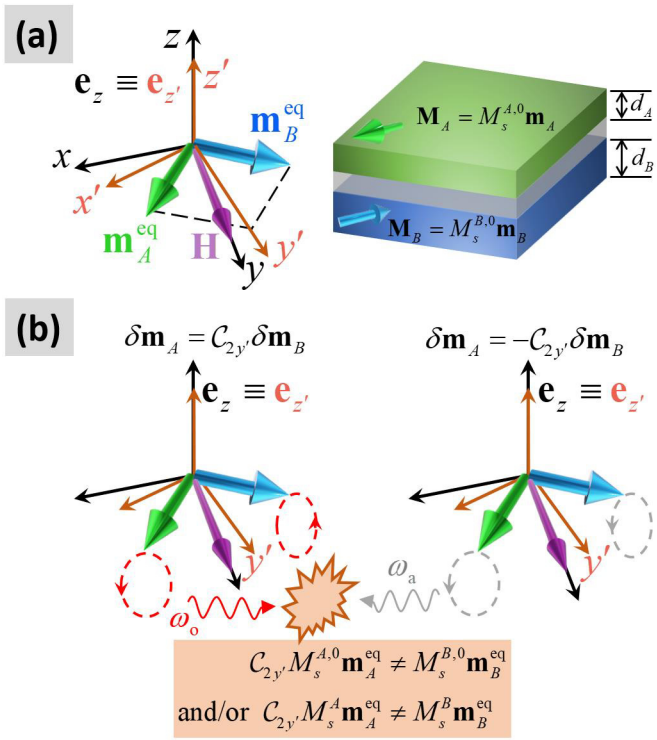

FIG. 1. (a) Sketch of a typical SAF with saturation magnetization $M_s^{A(B),0}$ and thickness $d_{A(B)}$ in its two FM sublayers. The macrospins ($\mathbf{m}_A$ and $\mathbf{m}_B$) of the two sublayers are coupled antiferromagnetically and tilted at equilibrium as $\mathbf{m}_A^{eq}$ and $\mathbf{m}_B^{eq}$. The unit vectors of the new $x'y'z$ coordinate system are: $\mathbf{e}_{x'} \parallel \mathbf{m}_A^{eq} - \mathbf{m}_B^{eq}$, $\mathbf{e}_{y'} \parallel \mathbf{m}_A^{eq} + \mathbf{m}_B^{eq}$, and $\mathbf{e}_z$ remains unchanged. (b) Sketch of magnon-magnon coupling between in-phase and out-of-phase modes. This coupling comes from the breaking rotation symmetry of magnetostatics and/or magnetization under $\mathcal{C}_{2y'}$ ($\mathcal{C}_{2y'}M_s^{A,0}\mathbf{m}_A^{eq} \neq M_s^{B,0}\mathbf{m}_B^{eq}$ and/or $\mathcal{C}_{2y'}M_s^{A}\mathbf{m}_A^{eq} \neq M_s^{B}\mathbf{m}_B^{eq}$).

The rest of this paper is organized as follows. In Sec. II, we briefly introduce the modelization of SAFs. In Sec. III, the static magnetization configuration of a SAF under dc in-plane magnetic fields is presented. After that, the dynamical response of magnetization system to external rf stimuli (i.e., FMR spectra) is provided in Sec. IV, which is the central result of this work. A general theory is proposed first, then applied to two typical cases of intrinsic SB and compared with existing experimental data to verify the validity. Finally, discussions and summary of this work are provided in the last two sections, respectively.

II. MODEL AND METHOD

The SAF system under consideration is sketched in Fig. 1(a). The saturation magnetization and thickness of the upper (lower) FM sublayer are $M_s^{A,0}$ and d_A ($M_s^{B,0}$ and d_B), respectively. The crystalline anisotropy in both sublayers are neglected for simplicity. In typical SAFs, the FM intralayer nearest-neighbor exchange is much stronger than the interlayer AFM coupling, which lays the foundation of the "macrospin" hypothesis. By denoting the unit magnetization vectors within respective sublayers as $\mathbf{m}_A$ and $\mathbf{m}_B$, the total magnetic energy of the SAF can be written as

$$\begin{aligned}
E_{\text{tot}} &= \mathcal{E}_A \cdot (Sd_A) + \mathcal{E}_B \cdot (Sd_B) + E_{\text{AFM}},\\
\mathcal{E}_A &= -\mu_0 M_s^{A,0}\mathbf{m}_A \cdot \mathbf{H} + \frac{1}{2}\mu_0\left(M_s^{A,0}\mathbf{m}_A \cdot \mathbf{n}\right)^2,\\
\mathcal{E}_B &= -\mu_0 M_s^{B,0}\mathbf{m}_B \cdot \mathbf{H} + \frac{1}{2}\mu_0\left(M_s^{B,0}\mathbf{m}_B \cdot \mathbf{n}\right)^2,\\
E_{\text{AFM}} &= \frac{1}{2}\mu_0\left(Sd_A M_s^{A,0}\mathbf{m}_A\right)\cdot\left(\lambda_E M_s^{B,0}\mathbf{m}_B\right)\\
&\quad + \frac{1}{2}\mu_0\left(\lambda_E M_s^{A,0}\mathbf{m}_A\right)\cdot\left(Sd_B M_s^{B,0}\mathbf{m}_B\right)\\
&= \frac{1}{2}\mu_0\lambda_E S(d_A + d_B)M_s^{A,0}M_s^{B,0}\mathbf{m}_A \cdot \mathbf{m}_B. \qquad (1)
\end{aligned}$$

Here, $\mathcal{E}_{A,B}$ are the energy densities of the two FM sublayers, respectively. The SAF has an area S with the corresponding surface normal $\mathbf{n}$. The first term in each energy density is the Zeeman term under an uniform in-plane external field $\mathbf{H}$, and the second term represents an easy-plane anisotropy from the magnetostatic interaction of a thin-disk-shaped FM sublayer. In addition, the expression of AFM interlayer coupling (E_{AFM}) comes from the simple picture in which the magnetic moments in one sublayer can be viewed as sitting in the effective field from the other sublayer with the dimensionless effectiveness λ_E. In literatures, this term is also expressed via the "interlayer exchange energy per unit area" J_{IEC}[6,7,10,12,15,18,19,21]. Hence $\lambda_E = 2J_{\text{IEC}}/[\mu_0 M_s^{A,0}M_s^{B,0}(d_A + d_B)]$.

The definition of effective field is generalized to the "macrospin" version as $\mathbf{H}_{\text{eff}} = -\mu_0^{-1}\delta E/\delta(\mathbf{M}Sd)$ with E, $\mathbf{M}$, d, and S being the magnetic energy, macrospin vector, thickness and area of a certain film, respectively. The interlayer coupling field in each sublayer then reads $\mathbf{H}_{\text{AFM}}^{A(B)} = -\lambda_E M_s^{B(A)}\mathbf{m}_{B(A)}$ with the "thickness-modified saturation magnetization" of the respective sublayer defined as

$$M_s^A = \frac{d_A + d_B}{2d_B}M_s^{A,0}, \quad M_s^B = \frac{d_A + d_B}{2d_A}M_s^{B,0}. \qquad (2)$$

After neglecting the damping terms, the coupled Landau-Lifshitz-Gilbert (LLG) equations are

$$\begin{aligned}
\dot{\mathbf{m}}_A &= -\gamma\mathbf{m}_A \times \left[\mathbf{H} - \lambda_E M_s^B\mathbf{m}_B - M_s^{A,0}(\mathbf{m}_A \cdot \mathbf{n})\mathbf{n}\right] + \tau_A,\\
\dot{\mathbf{m}}_B &= -\gamma\mathbf{m}_B \times \left[\mathbf{H} - \lambda_E M_s^A\mathbf{m}_A - M_s^{B,0}(\mathbf{m}_B \cdot \mathbf{n})\mathbf{n}\right] + \tau_B,
\end{aligned} \qquad (3)$$

where an overdot means d/dt, $\gamma = \mu_0\gamma_e$ with μ_0 and γ_e being the vacuum permeability and electron gyromagnetic ratio, respectively. At last, $\tau_{A(B)}$ is the torque on $\mathbf{m}_{A(B)}$ which arises from the rf excitation fields.

III. MAGNETOSTATICS OF SAFS WITH INTRINSIC SB

In later sections, we will present a general theory describing the effects of intrinsic SB on magnon-magnon coupling, as well as the FMR spectroscopy. As preparation, in this section we calculate the equilibrium magnetization orientations under an in-plane dc magnetic field $\mathbf{H}$ with strength H. In the absence of $\mathbf{H}$, the magnetostatic interaction leaves $\mathbf{m}_A$ and $\mathbf{m}_B$ lying within the SAF plane. Furthermore, the AFM interlayer

coupling makes them point in opposite directions. First we construct the original Cartesian coordinate system ($\mathbf{e}_x$, $\mathbf{e}_y$, $\mathbf{e}_z$): $\mathbf{e}_z \equiv \mathbf{n}$, $\mathbf{e}_x = \mathbf{m}_A(\mathbf{H}=0)$, and $\mathbf{e}_y = \mathbf{e}_z \times \mathbf{e}_x$. When $\mathbf{H} = H\mathbf{e}_y$ is applied, in principle $\mathbf{m}_A$ and $\mathbf{m}_B$ are pulled away from $\pm\mathbf{e}_x$ but still in xy plane. Their final equilibrium states are denoted as $\mathbf{m}_A^{\rm eq}$ and $\mathbf{m}_B^{\rm eq}$, respectively. In addition, since the in-plane magnetic (either crystalline or shape) anisotropy is neglected, the "spin-flop" process doe not happen in this system. We then set ϕ_A (ϕ_B) as the angle that $\mathbf{m}_A^{\rm eq}$ ($\mathbf{m}_B^{\rm eq}$) rotates anticlockwise (clockwise) with respect to $\mathbf{e}_x$ ($-\mathbf{e}_x$). They can be explicitly solved from the static LLG equations as

$$\sin\phi_{A(B)} = \frac{(H/\lambda_E)^2 + [M_s^{A(B)}]^2 - [M_s^{B(A)}]^2}{2HM_s^{A(B)}/\lambda_E}. \tag{4}$$

Next we define a new $x'y'z$ coordinate system based on $\mathbf{m}_A^{\rm eq}$ and $\mathbf{m}_B^{\rm eq}$: $\mathbf{e}_{x'} \parallel \mathbf{m}_A^{\rm eq} - \mathbf{m}_B^{\rm eq}$, $\mathbf{e}_{y'} \parallel \mathbf{m}_A^{\rm eq} + \mathbf{m}_B^{\rm eq}$, and $\mathbf{e}_z$ remains unchanged. In principle, $\mathbf{e}_{y'}$ deviates from $\mathbf{e}_y$ due to the intrinsic SB. To ensure the noncollinearity of $\mathbf{m}_A^{\rm eq}$ and $\mathbf{m}_B^{\rm eq}$ which is crucial for the definition of $x'y'z$ coordinate system, the dc field strength H should be limited within the range $H_{\rm AFM} < |H| < H_{\rm FM}$ with $H_{\rm AFM} \equiv \lambda_E|M_s^A - M_s^B|$ and $H_{\rm FM} \equiv \lambda_E(M_s^A + M_s^B)$. For $|H| \leqslant H_{\rm AFM}$ ($\geqslant H_{\rm FM}$), $\mathbf{m}_A^{\rm eq}$ and $\mathbf{m}_B^{\rm eq}$ point in the opposite (same) direction thus the SAF falls into AFM (FM) state. Then we denote $\mathcal{C}_{2y'}$ as the rotation operator which rotates vectors around the y' axis by 180°. Obviously, $\mathcal{C}_{2y'}^2 = 1$ and $\mathcal{C}_{2y'}\mathbf{m}_{A(B)}^{\rm eq} = \mathbf{m}_{B(A)}^{\rm eq}$. However, since $M_s^{A,0} \neq M_s^{B,0}$ and/or $d_A \neq d_B$, the joint operation of $\mathcal{C}_{2y'}$ and A-B sublayer exchange is no longer a symmetric operation of the entire SAF. This is the fundamental source of magnon-magnon coupling in SAFs with intrinsic SB, which greatly enriches the FMR spectra.

IV. MAGNON-MAGNON COUPLING AND FMR SPECTRA UNDER INTRINSIC SB

A. General theory

When a rf field with frequency $f = \omega/2\pi$ is exerted, the magnetization vectors are excited to deviate from their equilibrium orientations and begin to vibrate slightly. We then expand $\mathbf{m}_{A(B)} = \mathbf{m}_{A(B)}^{\rm eq} + \delta\mathbf{m}_{A(B)}e^{i\omega t}$ and $\tau_{A(B)} = \tau_{A(B)}^0 e^{i\omega t}$. In addition, we introduce $\delta\mathbf{m}_\pm \equiv \delta\mathbf{m}_A \pm \mathcal{C}_{2y'}\delta\mathbf{m}_B$ as the magnetization responses with even and odd parity (under $\mathcal{C}_{2y'}$) to the torque terms $\tau_\pm = \tau_A^0 \pm \mathcal{C}_{2y'}\tau_B^0$. By putting them into Eq. (3), keeping up to linear-order terms and performing standard symmetrization operations, we get our central vectorial equations for the magnetization excitations $\delta\mathbf{m}_\pm$,

$$\begin{aligned} i\frac{\omega}{\gamma}\delta\mathbf{m}_\pm = \mathbf{m}_A^{\rm eq} \times \Big\{ &\frac{\lambda_E}{2}\big(M_s^A + M_s^B\big)(\delta\mathbf{m}_\pm \pm \mathcal{C}_{2y'}\delta\mathbf{m}_\pm) + \frac{\lambda_E}{2}\big(M_s^A - M_s^B\big)(\delta\mathbf{m}_\mp \pm \mathcal{C}_{2y'}\delta\mathbf{m}_\mp) \\ &+ \frac{M_s^{A,0} \pm M_s^{B,0}}{4}[\mathbf{e}_z\mathbf{e}_z\cdot + \mathcal{C}_{2y'}\mathbf{e}_z(\mathcal{C}_{2y'}\mathbf{e}_z)\cdot]\delta\mathbf{m}_+ + \frac{M_s^{A,0} \pm M_s^{B,0}}{4}[\mathbf{e}_z\mathbf{e}_z\cdot - \mathcal{C}_{2y'}\mathbf{e}_z(\mathcal{C}_{2y'}\mathbf{e}_z)\cdot]\delta\mathbf{m}_- \\ &+ \frac{M_s^{A,0} \mp M_s^{B,0}}{4}[\mathbf{e}_z\mathbf{e}_z\cdot + \mathcal{C}_{2y'}\mathbf{e}_z(\mathcal{C}_{2y'}\mathbf{e}_z)\cdot]\delta\mathbf{m}_- + \frac{M_s^{A,0} \mp M_s^{B,0}}{4}[\mathbf{e}_z\mathbf{e}_z\cdot - \mathcal{C}_{2y'}\mathbf{e}_z(\mathcal{C}_{2y'}\mathbf{e}_z)\cdot]\delta\mathbf{m}_+ \Big\} + \tau_\pm. \end{aligned} \tag{5}$$

Now $\delta\mathbf{m}_+$ and $\delta\mathbf{m}_-$ are coupled by intrinsic SB terms (proportional to $M_s^A - M_s^B$ and $M_s^{A,0} - M_s^{B,0}$), thus result in strong magnon-magnon interaction between the bare modes with even and odd parities.

Next we move to the $x'y'$ plane (identical to the original xy plane) where $\mathbf{m}_{A(B)}^{\rm eq}$ resides in and denote ϕ' as the angle between $\mathbf{m}_A^{\rm eq}$ and $\mathbf{e}_{x'}$ which satisfies $\cos 2\phi' = [(M_s^A)^2 + (M_s^B)^2 - (H/\lambda_E)^2]/(2M_s^AM_s^B)$. In the local coordinate system "($\mathbf{e}_{\mathbf{m}} \equiv \mathbf{m}_A^{\rm eq}$, $\mathbf{e}_{\phi'} \equiv \mathbf{e}_z \times \mathbf{e}_{\mathbf{m}}$, $\mathbf{e}_z$)", $\delta\mathbf{m}_\pm$ can be decomposed to $\delta\mathbf{m}_\pm = \delta m_{\pm,\phi'}\mathbf{e}_{\phi'} + \delta m_{\pm,z}\mathbf{e}_z$. In the basis of $(\delta m_{+,\phi'}, \delta m_{+,z}, \delta m_{-,\phi'}, \delta m_{-,z})^{\rm T}$, for homogeneous case ($\tau_\pm = 0$) the above coupled vectorial equations are transformed into their matrix-form counterpart:

$$i\frac{\omega}{\gamma}\begin{pmatrix}\delta m_{+,\phi'}\\ \delta m_{+,z}\\ \delta m_{-,\phi'}\\ \delta m_{-,z}\end{pmatrix} = \begin{pmatrix} 0 & -\overline{M}_s^0 & 0 & -\overline{M}_s^0\kappa_0 \\ 2\lambda_E\overline{M}_s\cos^2\phi' & 0 & 2\lambda_E\overline{M}_s\kappa\cos^2\phi' & 0 \\ 0 & -\overline{M}_s^0\kappa_0 - 2\lambda_E\overline{M}_s\kappa & 0 & -\overline{M}_s^0 - 2\lambda_E\overline{M}_s \\ 2\lambda_E\overline{M}_s\kappa\sin^2\phi' & 0 & 2\lambda_E\overline{M}_s\sin^2\phi' & 0 \end{pmatrix}\begin{pmatrix}\delta m_{+,\phi'}\\ \delta m_{+,z}\\ \delta m_{-,\phi'}\\ \delta m_{-,z}\end{pmatrix}. \tag{6}$$

in which $\overline{M}_s^0 = (M_s^{A,0} + M_s^{B,0})/2$ and $\overline{M}_s = (M_s^A + M_s^B)/2$ are respectively the average bare and "thickness-modified" saturation magnetizations, meantime $\kappa_0 = (M_s^{A,0} - M_s^{B,0})/(M_s^{A,0} + M_s^{B,0})$ and $\kappa = (M_s^A - M_s^B)/(M_s^A + M_s^B)$ describe the degree of asymmetry between the two FM sublayers.

Consequently, the secular equation of Eq. (6) becomes

$$\tilde{\omega}^4 - \left(\tilde{h}^2 + \mu\frac{1+\kappa_0\kappa}{2\lambda_E}\right)\tilde{\omega}^2 + \frac{2\lambda_E + \nu}{4\lambda_E^2}\big(1-\tilde{h}^2\big)\big(\tilde{h}^2 - \kappa^2\big) = 0, \tag{7}$$

with $\tilde{\omega} \equiv \omega/(\gamma H_{\rm FM})$, $\kappa < \tilde{h} \equiv H/H_{\rm FM} < 1$, $\mu = (M_s^{A,0} + M_s^{B,0})/(M_s^A + M_s^B)$, and $\nu = (M_s^{A,0}/M_s^A)\cdot(M_s^{B,0}/M_s^B)$. Generally, a gap appears as long as $\kappa_0^2 + \kappa^2 \neq 0$. By first fixing H and solving the above secular equation then further sweeping H, the entire FMR spectrum in the "$\omega \sim H$" space can be obtained. In Fig. 2, the dimensionless FMR spectra under different configurations are provided based on Eq. (7). In all calculations, saturation magnetizations and magnetic fields are in the unit of $M_s^{A,0}$ and ω is in the unit of $\gamma M_s^{A,0}$. In addition, $\lambda_E = 0.1$. In the absence of any SB, a mode crossing always exists (see gray dashed curves in Fig. 2). When any single type of intrinsic SB appears, an anticrossing

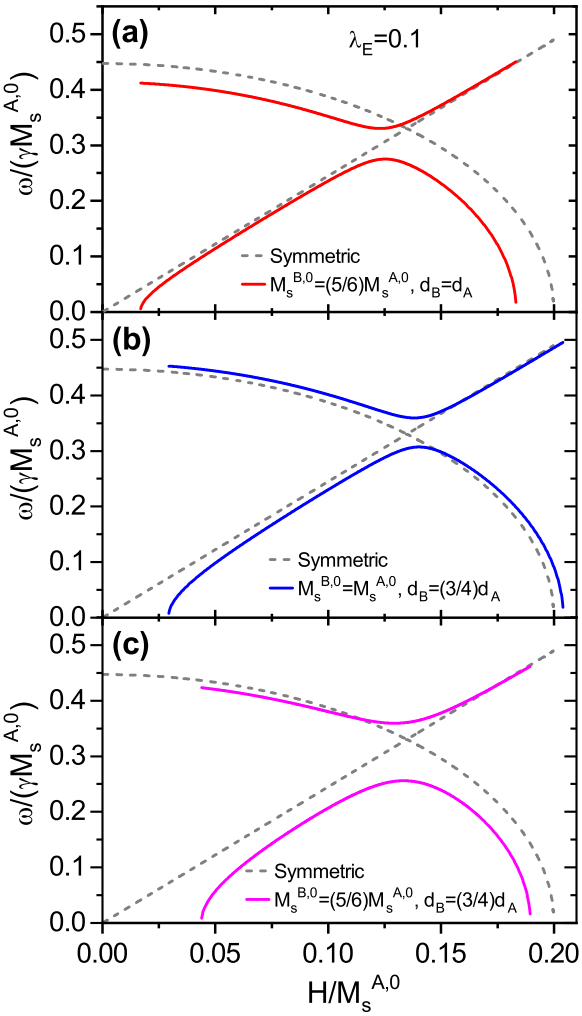

FIG. 2. Anticrossing gap opening when intrinsic SB emerges. In all calculations based on Eq. (7), $\lambda_E = 0.1$ and $M_s^{A,0}$ is taken as the unit of saturation magnetizations and magnetic fields. ω is in the unit of $\gamma M_s^{A,0}$. The inequalities of (a) bare saturation magnetization and (b) sublayer thickness are two sources of intrinsic SB. Each has been first independently shifted away from the symmetrical configuration (red and blue curves) in (a) and (b), and then together (magenta curve) in (c).

gap emerges. While both coexist, the gap width is greatly enlarged.

To acquire clearer physics meantime provide more convenient fitting tools for experiments, in the following we focus on two special cases and present more details about the anticrossing gap.

B. Same thickness but different material

In the first case, the two FM sublayers have the same thickness ($d_A = d_B$) but are made of different FM materials ($M_s^{A,0} \neq M_s^{B,0}$). Then $M_s^{A(B)} = M_s^{A(B),0}$, thus $\mu = \nu = 1$ and $\kappa_0 = \kappa \neq 0$. Similar to MacNeill *et al.* in 2019 [27], now the secular equation (7) can be rewritten into the eigenvalue problem of a 2×2 matrix as

$$\begin{vmatrix} \tilde{\omega}_a^2(\tilde{h}) - \tilde{\omega}^2 & \tilde{\Delta}^2 \\ \tilde{\Delta}^2 & \tilde{\omega}_o^2(\tilde{h}) - \tilde{\omega}^2 \end{vmatrix} = 0. \tag{8}$$

Here, $\tilde{\omega}_a = \sqrt{1 + (2\lambda_E)^{-1}}\tilde{h}$ and $\tilde{\omega}_o = [(1+\kappa^2)(1 - \tilde{h}^2)/(2\lambda_E) + (\kappa^2\tilde{h}^2)/(2\lambda_E)]^{1/2}$ are the bare in-phase (acoustic) and out-of-phase (optical) mode frequencies, respectively. Meantime $\tilde{\Delta} = [(2\lambda_E + 1)\kappa^2/(4\lambda_E^2)]^{1/4}$ describes the *dc-field-independent* magnon-magnon coupling strength. This is totally different from what has been reported in symmetrical FeCoB/Ru/FeCoB SAFs [20] or double-layered $CrCl_3$ system [27] where the magnon-magnon coupling strength is linearly proportional to the strength of oblique dc magnetic fields. The reason lies in the fact that the driving factor of magnon-magnon coupling therein is extrinsic and will disappear once the out-of-plane component of the external field is absent. While in our case, the driving factor is the intrinsic SB which always exists and is irrelevant to external stimuli.

When $|\kappa| \ll 1$ (nearly symmetric), $\tilde{\Delta}$ is negligible thus the solution of Eq. (8) are approximately $\tilde{\omega} \approx \tilde{\omega}_a$ and $\tilde{\omega} \approx \tilde{\omega}_o$. For finite κ, when $\tilde{h}$ is close to κ or 1, the solutions of Eq. (8) only deviate slightly from $\tilde{\omega}_a$ and $\tilde{\omega}_o$. When the optical and acoustic modes get closer in frequency, they will be hybridized by $\tilde{\Delta}$ term and thus a gap is opened. Direct calculations yield that this gap is an indirect gap (see Appendix A): the minimum $\tilde{\omega}_{up}^{min}$ (maximum $\tilde{\omega}_{down}^{max}$) of the "up (down)" branch takes place at $\tilde{h}_{up}^{min}$ ($\tilde{h}_{down}^{max}$), where $\tilde{h}_{up}^{min} \neq \tilde{h}_{down}^{max}$ for nonzero κ. The corresponding dimensionless gap width reads $\delta\tilde{\omega} = |\kappa|\sqrt{(2\lambda_E + 1)/[\lambda_E(\lambda_E + 1)]}$. Interestingly, the real gap width $\delta\tilde{\omega}$ is linear to $|\kappa|$ (degree of asymmetry between the two FM sublayers), which is different from the square-root dependence of the coupling $\tilde{\Delta}$ on κ. This is the direct consequence of indirect-gap opening where the gap width enlargement should be proportional to the square of the off-diagonal coupling term. Alternatively, in most existing works the magnon-magnon coupling strength $g_c/2\pi$ is obtained as half of the minimal frequency spacing (i.e., the gap size in $f \sim H$ spectrum) [18,27,29]. This comes from the "direct-gap opening" hypothesis in which the gap width is approximately twice of the off-diagonal coupling term. In summary, in SAFs with two inhomogeneous FM sublayers, the gap width takes square rather than linear dependence on the off-diagonal coupling term due to the indirect nature of the gap. Therefore the measuring method of magnon-magnon coupling strength in SAFs may need to be recalibrated case by case.

In Fig. 3, we plot the dependence of magnon-magnon coupling strength on gap width for different gap openings. For indirect gaps, $\tilde{\Delta} = \sqrt{\Delta\tilde{\omega} \cdot [(\lambda_E + 1)/(4\lambda_E)]}^{1/4}$ while for direct ones $\tilde{\Delta} = \Delta\tilde{\omega}/2$. We set $\lambda_E = 0.1$ and $0 < \Delta\tilde{\omega} < 1$, which are reasonable in real SAFs. Obviously, for the same gap width the magnon-magnon coupling strength for indirect case is much stronger than direct case. This implies higher efficiency of inducing magnon-magnon coupling in inhomogeneous SAFs. At last, by recalling the definitions of $\tilde{\omega}$ and κ,

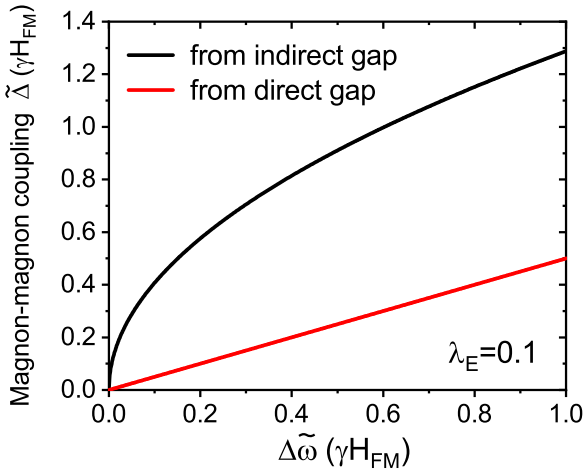

FIG. 3. Dependence of magnon-magnon coupling strength $\tilde{\Delta}$ on gap width $\Delta\tilde{\omega}$ for different types of gap opening. Both are in the unit of $\gamma H_{\rm FM}$ and $\lambda_E = 0.1$. Black (red) curve comes from indirect (direct) gap.

we get the dimensional gap width

$$\delta f = \sqrt{\frac{\lambda_E(2\lambda_E+1)}{\lambda_E+1}}\frac{\gamma}{2\pi}|M_s^{A,0} - M_s^{B,0}|, \tag{9}$$

which should be more useful for experimental physicists. Clearly, the AFM interlayer coupling and the inhomogeneity of sublayers are both crucial for the gap opening. On the other hand, we know that it is very difficult to prepare inhomogeneous SAFs ($M_s^{A,0} \neq M_s^{B,0}$) experimentally, however this issue is worth exploring further and Eq. (9) should help to reveal interesting physics.

C. Same material but different thickness

Another interesting case is that the two FM sublayers are made of the same material ($M_s^{A,0} = M_s^{B,0}$) but have different thickness ($d_A \neq d_B$), which is the most common choice in real experiments. Accordingly $\kappa_0 = 0$, $\kappa = (d_A - d_B)/(d_A + d_B)$ and $\mu = \nu = 1 - \kappa^2$. Now Eq. (7) can not be reorganized to the 2×2 matrix form as that in Eq. (8). However, similar calculus shows that now the gap is also indirect. The new extremum, extremum locations and the gap width become more complicated (see Appendix B), and we then focus on the situation where $|\kappa| \ll 1$. After standard linearization operation, the gap width is approximated to another linear dependence on $|\kappa|$ as $|\kappa|[(2\lambda_E+1)/(\lambda_E+1)]^{3/2}/(2\sqrt{\lambda_E})$. Back to dimensional form, we have

$$\delta f' \approx \frac{\sqrt{\lambda_E}}{2}\left(\frac{2\lambda_E+1}{\lambda_E+1}\right)^{\frac{3}{2}}\frac{|1-(d_B/d_A)^2|}{2(d_B/d_A)}\frac{\gamma}{2\pi}M_s^{A,0}. \tag{10}$$

Equation (10) can be directly compared with existing experiments in asymmetrical NiFe/Ru/NiFe SAFs [16,17]. For NiFe(13.6 nm)/Ru($t_{\rm Ru}$)/NiFe(27.2 nm) SAFs in Ref. [16], we choose $t_{\rm Ru} = 4.7$ Å as an example. By taking $M_s^{A,0} = 860\,{\rm kA\,m^{-1}}$ and $J_{\rm IEC} \approx |J_1| = 286\ \mu{\rm J\,m^{-2}}$, we get $\lambda_E \approx 0.015$ and $\delta f' \approx 1.4$ GHz. While for $Ni_{80}Fe_{20}$(200 Å)/Ru($t_{\rm Ru}$)/$Ni_{80}Fe_{20}$(100 Å) SAFs in Ref. [17], the magnetic parameters for $t_{\rm Ru} = 3.3$ Å are $M_s^{A,0} = 720\,{\rm kA\,m^{-1}}$ and $J_{\rm IEC} \approx 154\ \mu{\rm J\,m^{-2}}$. These lead to $\lambda_E \approx 0.016$ and $\delta f' \approx 1.2$ GHz. For other Ru thickness, similar calculations can be performed and all results show agreement between analytic and experimental data.

Interestingly, in FeCoB/Ru/FeCoB SAFs, we can acquire larger λ_E, although nearly all existing published experiments are performed in symmetrical cases [18–21]. For symmetrical FeCoB thickness being 15[18,19], 3 [20], and 5 nm [21], the respective λ_E are estimated to be 0.033, 0.093 and 0.119(0.141) (two samples therein). Combined with larger saturation magnetization of FeCoB, asymmetrical FeCoB/Ru/FeCoB SAFs are expected to open larger indirect gaps. Our results provide the possibility that by appropriately designing the thickness ratio of two FeCoB sublayers, greater gap can be opened which indicates stronger magnon-magnon coupling. On the other hand, although the magnon-magnon coupling strength can not be explicitly written out as the inhomogeneity case in Sec. IV B, the indirect nature of the gap here makes it also have square-root dependence on the asymmetry degree $|\kappa|$ at least when $|\kappa| \ll 1$ due to the linear dependence of gap width on $|\kappa|$ at that time.

V. DISCUSSIONS

At the end of this work, several points need to be clarified. First, in this work the crystalline anisotropy has been neglected because of two reasons: (i) in most existing experimental setups, the FM sublayers of SAFs are made from soft magnetic materials which can be viewed as isotropic; (ii) the explicit orientations of $\mathbf{m}_A^{\rm eq}$ and $\mathbf{m}_B^{\rm eq}$ can hardly be obtained analytically if the in-plane crystalline anisotropy is considered (even for the simplest uniaxial case), but they are crucial for obtaining the vectorial LLG equations and then the secular equations for FMR frequencies. For the above reasons, in this work, we choose the isotropic case for simplicity, but it can cover the vast majority of experimental data. Note that our analytics also holds for perpendicular-magnetic-anisotropy case as long as we change $M_s^{A(B),0}$ to $M_s^{A(B),0} - H_K^{A(B)}$ in Eq. (3) where $H_K^{A(B)}$ is the out-of-plane anisotropic field in the respective sublayer. Another neglected term is the Gilbert damping term. In most investigations of spin wave, the damping term is dropped off when only the resonance spectrum is under consideration. However when the linewidth is also of interest, the damping process should be included in Eq. (5) by a respective term $i\omega\alpha\mathbf{m}_A^{\rm eq} \times \delta\mathbf{m}_\pm$ with α being the Gilbert damping coefficient [27].

Second, in principle the dimensionless parameter λ_E describes the AFM interacting effectiveness of the macrospin in one sublayer to the other, thus should be independent on the thickness of two sublayers. This equivalently means that $J_{\rm IEC}$ is a "bulk" parameter thus should be proportional to the total thickness of the two sublayers. However, in real experiments, the atomic layers of the two FM sublayers closest to the spacer provide most of the energy contribution to $J_{\rm IEC}$. In addition, the thicker the two sublayers are, the farther the system deviates from the "macropin" hypothesis. The combination of these factors makes the experimental $J_{\rm IEC}$ in thick SAFs (especially in some early experiments) almost a constant value

and independent on the total thickness of the two sublayers. Consequently, λ_E could no longer be a constant parameter and inversely proportional to $d_A + d_B$. Accordingly, all the analytics in the main text should be recalibrated. Fortunately, in recent experiments, the thickness of SAF sublayers have been reduced to less than 10 nanometers, where the "macropin" hypothesis holds and almost all atomic layers contribute to J_{IEC}. Therefore λ_E is nearly constant and our present theory holds.

Third, in the main text, we only considered the intrinsic SB and constructed a theory for describing the resulting magnon-magnon coupling. In fact, an unified theoretical framework which combines the effects of both intrinsic and extrinsic (originating from out-of-plane dc magnetic field components) SB can be proposed. The details have been provided in Appendix C. Here we emphasize the difference between the mechanisms of inducing magnon-magnon coupling by extrinsic and intrinsic SB. For extrinsic SB, the breaking rotation symmetry of hard axis **n** (from magnetostatic interaction) with respect to the pulled up rotation-symmetry axis (due to oblique dc fields) is the basic reason. While for intrinsic SB, the new rotation axis is still in the SAF plane but the entire magnetic layout (including magnetization and magnetostatics) is no longer unchanged under the twofold rotation. The entanglement between magnetization vibrations with opposite parity results in the strong magnon-magnon coupling thus greatly affects the FMR spectroscopy of SAFs.

VI. SUMMARY

In summary, we have proposed a simple but revealing theory for understanding the rich structure of FMR spectroscopy in asymmetrical SAFs, where the twofold rotation symmetry of either the magnetization or magnetostatics fails. The intrinsic SB in SAFs causes entanglement between magnetization vibrations with opposite parity, thus excites strong magnon-magnon coupling between the bare in-phase and out-of-phase modes, then eventually results in the anticrossing gap in microwave absorption spectroscopy. Furthermore, the indirect nature of this gap leads to square (rather than linear) dependence of gap width on magnon-magnon coupling strength. This new picture helps to understand the rich experimental data of FMR spectra for existing SAFs and future measurements on other SAF or SAF-like systems.

ACKNOWLEDGMENTS

M.L. acknowledges supports from the National Natural Science Foundation of China (Grant No. 11947023), the Project of Hebei Province Higher Educational Science and Technology Program (QN2019309) and the PhD Research Startup Foundation of Shijiazhuang University (20BS022). J.L. is funded by the Natural Science Foundation for Distinguished Young Scholars of Hebei Province of China (S&T Program of Hebei, Grant No. A2019205310). W.H. is supported by the National Natural Science Foundation of China (Grant No. 51871235).

APPENDIX A: DETAILS FOR "SAME THICKNESS BUT DIFFERENT MATERIAL"

In this case, $d_A = d_B$ but $M_s^{A,0} \neq M_s^{B,0}$. Then $M_s^{A(B)} = M_s^{A(B),0}$, thus $\mu = \nu = 1$, $\kappa_0 = \kappa \neq 0$. The secular equation in Eq. (7) of the main text is simplified to

$$\tilde{\omega}^4 - \left(\tilde{h}^2 + \frac{1+\kappa^2}{2\lambda_E}\right)\tilde{\omega}^2 + \frac{2\lambda_E+1}{4\lambda_E^2}\left(1-\tilde{h}^2\right)\left(\tilde{h}^2-\kappa^2\right) = 0. \tag{A1}$$

The two branches turn out to be

$$\tilde{\omega}_{\mathrm{up,down}} = \frac{1}{2\sqrt{\lambda_E}} \cdot \sqrt{\left[2\lambda_E\tilde{h}^2 + (1+\kappa^2)\right] \pm \sqrt{\left[2(\lambda_E+1)\tilde{h}^2 - (1+\kappa^2)\right]^2 + 4(2\lambda_E+1)\kappa^2}}, \tag{A2}$$

where "+(−)" means up (down) branch. Direct calculation yields that the extremum and extremum locations are as follows:

$$\tilde{\omega}_{\mathrm{up(down)}}^{\mathrm{min(max)}} = \sqrt{\frac{2\lambda_E+1}{4\lambda_E(\lambda_E+1)}}(1 \pm |\kappa|) \tag{A3}$$

at

$$\tilde{h}_{\mathrm{up(down)}}^{\mathrm{min(max)}} = \sqrt{\frac{1+\kappa^2 \mp 2\lambda_E|\kappa|}{2(\lambda_E+1)}}. \tag{A4}$$

For nonzero κ, $\tilde{h}_{\mathrm{up}}^{\mathrm{min}} \neq \tilde{h}_{\mathrm{down}}^{\mathrm{max}}$ thus resulting in the dimensionless indirect gap:

$$\delta\tilde{\omega} = \tilde{\omega}_{\mathrm{up}}^{\mathrm{min}} - \tilde{\omega}_{\mathrm{down}}^{\mathrm{max}} = \sqrt{\frac{2\lambda_E+1}{\lambda_E(\lambda_E+1)}}|\kappa|. \tag{A5}$$

Note that $\tilde{\omega} = \omega/[\gamma\lambda_E(M_s^A + M_s^B)]$ and $\kappa = (M_s^A - M_s^B)/(M_s^A + M_s^B)$, then finally we get the dimensional gap width as shown in Eq. (9) in the main text, which takes place around $H \approx (\tilde{h}_{\mathrm{up}}^{\mathrm{min}} + \tilde{h}_{\mathrm{down}}^{\mathrm{max}})H_{\mathrm{FM}}/2$ and $f \approx (\tilde{\omega}_{\mathrm{up}}^{\mathrm{min}} + \tilde{\omega}_{\mathrm{down}}^{\mathrm{max}})\gamma H_{\mathrm{FM}}/(4\pi)$.

APPENDIX B: DETAILS FOR "SAME MATERIAL BUT DIFFERENT THICKNESS"

Now $M_s^{A,0} = M_s^{B,0}$ but $d_A \neq d_B$. Thus $\kappa_0 = 0$, $\kappa = (d_A - d_B)/(d_A + d_B)$ and $\mu = \nu = 1 - \kappa^2$. The secular equation in Eq. (7) of the main text becomes

$$\tilde{\omega}^4 - \Big(\tilde{h}^2 + \frac{\mu}{2\lambda_E}\Big)\tilde{\omega}^2 + \frac{2\lambda_E + \mu}{4\lambda_E^2}\big(1 - \tilde{h}^2\big)\big(\tilde{h}^2 + \mu - 1\big) = 0. \tag{B1}$$

The two branches can be directly calculated as

$$\tilde{\omega}_{\text{up,down}} = \frac{1}{\sqrt{2}} \cdot \sqrt{\Big(\tilde{h}^2 + \frac{\mu}{2\lambda_E}\Big) \pm \frac{\sqrt{\lambda_E^2 + 2\lambda_E + \mu}}{\lambda_E} \sqrt{\Big[\tilde{h}^2 - \frac{(2\lambda_E + \mu)(2 - \mu) - \mu\lambda_E}{2(\lambda_E^2 + 2\lambda_E + \mu)}\Big]^2 + \frac{(1 - \mu)(2\lambda_E + \mu)^3}{4(\lambda_E^2 + 2\lambda_E + \mu)^2}}}, \tag{B2}$$

with "+(−)" indicating up (down) branch. After standard calculus, the extremum and corresponding locations are

$$\tilde{\omega}_{\text{up(down)}}^{\text{min(max)}} = \frac{1}{2}\sqrt{\frac{(2\lambda_E + \mu)\big[(2\lambda_E + \mu)(1 \pm \sqrt{1 - \mu}) - \mu\lambda_E\big]}{\lambda_E(\lambda_E^2 + 2\lambda_E + \mu)}} \tag{B3}$$

at

$$\tilde{h}_{\text{up(down)}}^{\text{min(max)}} = \sqrt{\frac{(2\lambda_E + \mu)(2 - \mu \mp \lambda_E\sqrt{1 - \mu}) - \mu\lambda_E}{2(\lambda_E^2 + 2\lambda_E + \mu)}}. \tag{B4}$$

The dimensionless indirect gap then takes the following form:

$$\delta\tilde{\omega} = \tilde{\omega}_{\text{up}}^{\text{min}} - \tilde{\omega}_{\text{down}}^{\text{max}} = \frac{2\lambda_E + \mu}{2\sqrt{\lambda_E(\lambda_E^2 + 2\lambda_E + \mu)}}\left(\sqrt{1 - \frac{\mu\lambda_E}{2\lambda_E + \mu} + \sqrt{1 - \mu}} - \sqrt{1 - \frac{\mu\lambda_E}{2\lambda_E + \mu} - \sqrt{1 - \mu}}\right), \tag{B5}$$

which shows a complicated dependence on the asymmetry degree $|\kappa| = \sqrt{1 - \mu}$. To acquire a more clear insight of the gap width dependence on $|\kappa|$, we choose the "small-κ" limit as an example, which corresponds to the case where there is not much difference between the thickness of two FM sublayers. After standard linearization operation and only keeping the linear terms of κ, we reach the following result:

$$\delta\tilde{\omega} = \tilde{\omega}_{\text{up}}^{\text{min}} - \tilde{\omega}_{\text{down}}^{\text{max}} \approx \frac{1}{2\sqrt{\lambda_E}}\left(\frac{2\lambda_E + 1}{\lambda_E + 1}\right)^{\frac{3}{2}}|\kappa| \tag{B6}$$

for $|\kappa| \ll 1$. Remembering that $\tilde{\omega} = \omega/[\gamma\lambda_E(M_s^A + M_s^B)]$, $\kappa = (M_s^A - M_s^B)/(M_s^A + M_s^B)$ and the definitions of $M_s^{A(B)}$ in the main text, then the dimensional gap width takes the form in Eq. (10) of the main text, which also takes place around $H \approx (\tilde{h}_{\text{up}}^{\text{min}} + \tilde{h}_{\text{down}}^{\text{max}})H_{\text{FM}}/2$ and $f \approx (\tilde{\omega}_{\text{up}}^{\text{min}} + \tilde{\omega}_{\text{down}}^{\text{max}})\gamma H_{\text{FM}}/(4\pi)$.

APPENDIX C: UNIFIED THEORY INCLUDING OBLIQUE DC FIELDS

In this Appendix, we provide a unified theory that includes both an oblique dc magnetic field $\mathbf{H}$ (with strength H) and intrinsic SB effects. As preparation, we redefine the global Cartesian coordinate system $(\mathbf{e}_x, \mathbf{e}_y, \mathbf{e}_z)$ as follows: $\mathbf{e}_z \equiv \mathbf{n}$ thus the oblique angle of $\mathbf{H}$ with respect to SAF plane is $\psi \equiv \sin^{-1}(\mathbf{e}_z \cdot \mathbf{H}/H)$ which satisfies $0 \leqslant \psi < \pi/2$, $\mathbf{e}_y$ is parallel to the in-plane field component $\mathbf{H} - H\sin\psi\mathbf{e}_z$, and $\mathbf{e}_x = \mathbf{e}_y \times \mathbf{e}_z$. As indicated in the main text, without $\mathbf{H}$ the unit magnetization vectors in the two sublayers orient oppositely in a certain in-plane direction in the absence of any in-plane anisotropy due to the AFM interlayer coupling. When $\mathbf{H}$ is applied, in principle, they are pulled out of xy plane and their final equilibrium states are denoted as $\mathbf{m}_A^{\text{eq}}$ and $\mathbf{m}_B^{\text{eq}}$, respectively. We then set $\theta_{A(B)}$ as their respective polar angles, and ϕ_A (ϕ_B) being the angle that in-plane component of $\mathbf{m}_A^{\text{eq}}$ ($\mathbf{m}_B^{\text{eq}}$) rotates anticlockwise (clockwise) with respect to $\mathbf{e}_x$ ($-\mathbf{e}_x$). These four angles can be explicitly solved as

$$\begin{aligned}
\cos\theta_{A(B)} &= \frac{M_s^{B(A),0}H\sin\psi}{\lambda_E\big(M_s^A M_s^{B,0} + M_s^B M_s^{A,0}\big) + M_s^{A,0}M_s^{B,0}}, \\
\sin\phi_{A(B)} &= \frac{\big(\frac{H}{\lambda_E}\cos\psi\big)^2 + [M_s^{A(B)}\sin\theta_{A(B)}]^2 - [M_s^{B(A)}\sin\theta_{B(A)}]^2}{2\frac{H}{\lambda_E}\cos\psi \cdot M_s^{A(B)}\sin\theta_{A(B)}}.
\end{aligned} \tag{C1}$$

Next we define a totally new $x'y'z'$ coordinate system based on $\mathbf{m}_A^{\text{eq}}$ and $\mathbf{m}_B^{\text{eq}}$: $\mathbf{e}_{x'} \parallel \mathbf{m}_A^{\text{eq}} - \mathbf{m}_B^{\text{eq}}$, $\mathbf{e}_{y'} \parallel \mathbf{m}_A^{\text{eq}} + \mathbf{m}_B^{\text{eq}}$, and $\mathbf{e}_{z'} \parallel \mathbf{m}_A^{\text{eq}} \times \mathbf{m}_B^{\text{eq}}$. The noncollinearity of $\mathbf{m}_A^{\text{eq}}$ and $\mathbf{m}_B^{\text{eq}}$ is crucial for the construction of new $x'y'z'$ coordinate system. This is equivalent to require $0 < |\sin\phi_{A(B)}| < 1$, i.e., $0 \leqslant H_{\text{AFM}} < |H| < H_{\text{FM}}$, in which $(H_{\text{AFM}})^2$ and $(H_{\text{FM}})^2$ are the two roots of the quadratic

equation $ax^2 - 2bx + c = 0$ with

$$a = \frac{\cos^4\psi}{\lambda_E^4} + \frac{\left[(M_s^A M_s^{B,0})^2 - (M_s^B M_s^{A,0})^2\right]^2 \sin^4\psi}{\left[\lambda_E\left(M_s^A M_s^{B,0} + M_s^B M_s^{A,0}\right) + M_s^{A,0} M_s^{B,0}\right]^4} + \frac{\left[(M_s^A M_s^{B,0})^2 + (M_s^B M_s^{A,0})^2\right] 2\sin^2\psi\cos^2\psi}{\left[\lambda_E^2\left(M_s^A M_s^{B,0} + M_s^B M_s^{A,0}\right) + \lambda_E M_s^{A,0} M_s^{B,0}\right]^2},$$

$$b = \frac{\left[(M_s^A)^2 + (M_s^B)^2\right]}{\lambda_E^2}\cos^2\psi + \frac{\left[(M_s^A)^2 - (M_s^B)^2\right]\left[(M_s^A M_s^{B,0})^2 - (M_s^B M_s^{A,0})^2\right]}{\left[\lambda_E\left(M_s^A M_s^{B,0} + M_s^B M_s^{A,0}\right) + M_s^{A,0} M_s^{B,0}\right]^2}\sin^2\psi,$$

$$c = \left[\left(M_s^A\right)^2 - \left(M_s^B\right)^2\right]^2. \tag{C2}$$

After constructing the new $x'y'z'$ coordinate system, the $\mathcal{C}_{2y'}$ operator remains its original physical meaning: it rotates vectors around the y' axis by 180°. Still, we take the combinations of magnetization vibrations in the two FM sublayers, $\delta\mathbf{m}_\pm = \delta\mathbf{m}_A \pm \mathcal{C}_{2y'}\delta\mathbf{m}_B$, as our central variables to obtain the FMR spectra. The resulting dynamical vectorial equations have the same form as that in Eq. (5) of the main text, however the physics embedded has been greatly enriched since now $\mathcal{C}_{2y'}\mathbf{e}_z \neq -\mathbf{e}_z$.

Accordingly, to obtain the matrix form of dynamical equations, we move again to the new $x'y'$ plane (now differs from the original xy plane) where $\mathbf{m}_{A(B)}^{\rm eq}$ reside in. In the local coordinate system "$(\mathbf{e}_\mathbf{m} \equiv \mathbf{m}_A^{\rm eq}, \mathbf{e}_{\phi'} \equiv \mathbf{e}_{z'} \times \mathbf{e}_\mathbf{m}, \mathbf{e}_{z'})$", $\delta\mathbf{m}_\pm$ can be decomposed to $\delta\mathbf{m}_\pm = \delta m_{\pm,\phi'}\mathbf{e}_{\phi'} + \delta m_{\pm,z'}\mathbf{e}_{z'}$. In the basis of $(\delta m_{+,\phi'}, \delta m_{+,z'}, \delta m_{-,\phi'}, \delta m_{-,z'})^{\rm T}$, for homogeneous case ($\tau_\pm = 0$) Eq. (5) in the main text is transformed into its matrix-form counterpart:

$$\mathrm{i}\frac{\omega}{\gamma}\begin{pmatrix}\delta m_{+,\phi'}\\ \delta m_{+,z'}\\ \delta m_{-,\phi'}\\ \delta m_{-,z'}\end{pmatrix} = \begin{pmatrix} p_1 & p_2 & p_3 & p_4\\ q_1 + 2\lambda_E\overline{M}_s\cos^2\phi' & -p_1 & q_2 + 2\lambda_E\overline{M}_s\kappa\cos^2\phi' & -p_3\\ p_3 & p_4 - 2\lambda_E\overline{M}_s\kappa & p_1 & p_2 - 2\lambda_E\overline{M}_s\\ q_2 + 2\lambda_E\overline{M}_s\kappa\sin^2\phi' & -p_3 & q_1 + 2\lambda_E\overline{M}_s\sin^2\phi' & -p_1\end{pmatrix}\begin{pmatrix}\delta m_{+,\phi'}\\ \delta m_{+,z'}\\ \delta m_{-,\phi'}\\ \delta m_{-,z'}\end{pmatrix}, \tag{C3}$$

in which $p_1 = \overline{M}_s^0(\cos\alpha\sin\phi' - \kappa_0\cos\beta\cos\phi')\cos\eta$, $p_2 = -\overline{M}_s^0\cos^2\eta$, $p_3 = \overline{M}_s^0(\kappa_0\cos\alpha\sin\phi' - \cos\beta\cos\phi')\cos\eta$, $p_4 = -\overline{M}_s^0\kappa_0\cos^2\eta$, $q_1 = [(p_1 - p_3)^2(p_4 + p_2) - (p_1 + p_3)^2(p_4 - p_2)]/[2(p_4^2 - p_2^2)]$, and $q_2 = [-(p_1 - p_3)^2(p_4 + p_2) - (p_1 + p_3)^2(p_4 - p_2)]/[2(p_4^2 - p_2^2)]$. In addition, $\cos\alpha$, $\cos\beta$ and $\cos\eta$ are the three cosines of $\mathbf{e}_z$ in the new $x'y'z'$ coordinate system: $\cos\alpha = (\cos\theta_A - \cos\theta_B)/(2\cos\phi')$, $\cos\beta = (\cos\theta_A + \cos\theta_B)/(2\sin\phi')$, and $\cos\eta = \sqrt{\sin^2\theta_A\sin^2\theta_B - (\cos\theta_A\cos\theta_B + \cos 2\phi')^2}/\sin 2\phi'$. At last, ϕ' is the angle between $\mathbf{m}_A^{\rm eq}$ and $\mathbf{e}_{x'}$ which satisfies $\cos 2\phi' = -\cos\theta_A\cos\theta_B + [(M_s^A\sin\theta_A)^2 + (M_s^B\sin\theta_B)^2 - (H\cos\psi/\lambda_E)^2]/(2M_s^A M_s^B)$. The corresponding secular equation then provide the FMR spectra of this SAF. In the most general case where $\kappa_0 \neq 0$, $\kappa \neq 0$ and $\psi > 0$, the secular equation can hardly be solved analytically. However, based on the above results numerical calculation can always be performed once we have knowledge on $M_s^{A(B),0}$, $d_{A(B)}$, λ_E, and ψ. When the out-of-plane components of external dc fields are absent, the unified theory presented above then falls back to the one provided in the main text.

[1] R. A. Duine, K.-J. Lee, S. S. P. Parkin, and M. D. Stiles, Nat. Phys. **14**, 217 (2018).

[2] T. Martin, M. Belmeguenai, M. Maier, K. Perzlmaier, and G. Bayreuther, J. Appl. Phys. **101**, 09C101 (2007).

[3] T. Seki, H. Tomita, A. A. Tulapurkar, M. Shiraishi, T. Shinjo, and Y. Suzuk, Appl. Phys. Lett. **94**, 212505 (2009).

[4] D. E. Gonzalez-Chavez, R. Dutra, W. O. Rosa, T. L. Marcondes, A. Mello, and R. L. Sommer, Phys. Rev. B **88**, 104431 (2013).

[5] A. A. Timopheev, Y. G. Pogorelov, S. Cardoso, P. P. Freitas, G. N. Kakazei, and N. A. Sobolev, Phys. Rev. B **89**, 144410 (2014).

[6] K. Tanaka, T. Moriyama, M. Nagata, T. Seki, K. Takanashi, S. Takahashi, and T. Ono, Appl. Phys. Express **7**, 063010 (2014).

[7] H. Yang, Y. Li, and W. E. Bailey, Appl. Phys. Lett. **108**, 242404 (2016).

[8] S. Li, Q. Li, J. Xu, S. Yan, G.-X. Miao, S. Kang, Y. Dai, J. Jiao, and Y. Lü, Adv. Funct. Mater. **26**, 3738 (2016).

[9] C. Wang, S. Zhang, S. Qiao, H. Du, X. Liu, R. Sun, X.-M. Chu, G.-X. Miao, Y. Dai, S. Kang, S. Yan, and S. Li, Appl. Phys. Lett. **112**, 192401 (2018).

[10] W. Wang, P. Li, C. Cao, F. Liu, R. Tang, G. Chai, and C. Jiang, Appl. Phys. Lett. **113**, 042401 (2018).

[11] W. J. Kong, C. H. Wan, B. S. Tao, C. Fang, L. Huang, C. Y. Guo, M. Irfan, and X. F. Han, Appl. Phys. Lett. **113**, 162402 (2018).

[12] A. Kamimaki, S. Iihama, T. Taniguchi, and S. Mizukami, Appl. Phys. Lett. **115**, 132402 (2019).

[13] R. Y. Chen, R. Q. Zhang, L. Y. Liao, X. Z. Chen, Y. J. Zhou, Y. D. Gu, M. S. Saleem, X. F. Zhou, F. Pan, and C. Song, Appl. Phys. Lett. **115**, 132403 (2019)

[14] S. Sorokin, R. A. Gallardo, C. Fowley, K. Lenz, A. Titova, G. Y. P. Atcheson, G. Dennehy, K. Rode, J. Fassbender, J. Lindner, and A. M. Deac, Phys. Rev. B **101**, 144410 (2020).

[15] A. Kamimaki, S. Iihama, K. Z. Suzuki, N. Yoshinaga, and S. Mizukami, Phys. Rev. Appl. **13**, 044036 (2020).

[16] M. Belmeguenai, T. Martin, G. Woltersdorf, G. Bayreuther, V. Baltz, A. K. Suszka, and B. J. Hickey, J. Phys.: Condens. Matter **20**, 345206 (2008).

[17] X. M. Liu, H. T. Nguyen, J. Ding, M. G. Cottam, and A. O. Adeyeye, Phys. Rev. B **90**, 064428 (2014).

[18] Y. Shiota, T. Taniguchi, M. Ishibashi, T. Moriyama, and T. Ono, Phys. Rev. Lett. **125**, 017203 (2020).

[19] M. Ishibashi, Y. Shiota, T. Li, S. Funada, T. Moriyama, and T. Ono, Sci. Adv. **6**, eaaz6931 (2020).

[20] A. Sud, C. W. Zollitsch, A. Kamimaki, T. Dion, S. Khan, S. Iihama, S. Mizukami, and H. Kurebayashi, Phys. Rev. B **102**, 100403(R) (2020).
[21] H. J. Waring, N. A. B. Johansson, I. J. Vera-Marun, and T. Thomson, Phys. Rev. Appl. **13**, 034035 (2020).
[22] T. Kampfrath, A. Sell, G. Klatt, A. Pashkin, S. Mhrlein, T. Dekorsy, M. Wolf, M. Fiebig, A. Leitenstorfer, and R. Huber, Nat. Photonics **5**, 31 (2011).
[23] S. Baierl, J. H. Mentink, M. Hohenleutner, L. Braun, T.-M. Do, C. Lange, A. Sell, M. Fiebig, G. Woltersdorf, T. Kampfrath, and R. Huber, Phys. Rev. Lett. **117**, 197201 (2016).
[24] M. A. Ruderman and C. Kittel, Phys. Rev. **96**, 99 (1954).
[25] Y. Yafet, J. Appl. Phys. **61**, 4058 (1987).
[26] P. Bruno and C. Chappert, Phys. Rev. Lett. **67**, 1602 (1991).
[27] D. MacNeill, J. T. Hou, D. R. Klein, P. Zhang, P. Jarillo-Herrero, and L. Liu, Phys. Rev. Lett. **123**, 047204 (2019).
[28] X.-X. Zhang, L. Li, D. Weber, J. Goldberger, K. F. Mak, and J. Shan, Nat. Mater. **19**, 838 (2020).
[29] L. Liensberger, A. Kamra, H. Maier-Flaig, S. Geprägs, A. Erb, S. T. B. Goennenwein, R. Gross, W. Belzig, H. Huebl, and M. Weiler, Phys. Rev. Lett. **123**, 117204 (2019).